

# Spectral properties of the soft excess pulsar RX J0059.2–7138 during its 2013 outburst

L. Sidoli,<sup>1\*</sup> N. La Palombara,<sup>1</sup> P. Esposito,<sup>1,2</sup> A. Tiengo,<sup>3,1,4</sup> S. Mereghetti,<sup>1</sup>

<sup>1</sup>*INAF, Istituto di Astrofisica Spaziale e Fisica Cosmica, Via E. Bassini 15, I-20133 Milano, Italy*

<sup>2</sup>*Harvard-Smithsonian Center for Astrophysics, 60 Garden Street, Cambridge, MA 02138, USA*

<sup>3</sup>*IUSS, Istituto Universitario di Studi Superiori, piazza della Vittoria 15, I-27100 Pavia, Italy*

<sup>4</sup>*INFN, Sezione di Pavia, via A. Bassi 6, I-27100 Pavia, Italy*

Accepted 2015 March 13. Received 2015 March 13; in original form 2015 February 18

## ABSTRACT

We report on an X–ray observation of the Be X–ray Binary Pulsar RX J0059.2–7138, performed by *XMM-Newton* in March 2014. The 19 ks long observation was carried out about three months after the discovery of the latest outburst from this Small Magellanic Cloud transient, when the source luminosity was  $L_X \sim 10^{38}$  erg s<sup>−1</sup>. A spin period of  $P_{\text{spin}} = 2.762383(5)$  s was derived, corresponding to an average spin-up of  $\dot{P}_{\text{spin}} = -(1.27 \pm 0.01) \times 10^{-12}$  s s<sup>−1</sup> from the only previous period measurement, obtained more than 20 years earlier. The time-averaged continuum spectrum (0.2–12 keV) consisted of a hard power-law (photon index  $\sim 0.44$ ) with an exponential cut-off at a phase-dependent energy ( $\sim 20$ –50 keV) plus a significant soft excess below  $\sim 0.5$  keV. In addition, several features were observed in the spectrum: an emission line at 6.6 keV from highly ionized iron, a broad feature at 0.9–1 keV likely due to a blend of Fe L-shell lines, and narrow emission and absorption lines consistent with transitions in highly ionized oxygen, nitrogen and iron visible in the high resolution RGS data (0.4–2.1 keV). Given the different ionization stages of the narrow line components, indicative of photoionization from the luminous X–ray pulsar, we argue that the soft excess in RX J0059.2–7138 is produced by reprocessing of the pulsar emission in the inner regions of the accretion disc.

**Key words:** accretion - stars: neutron - X–rays: binaries - X–rays: individual (RX J0059.2–7138)

## 1 INTRODUCTION

The dominant component in the spectra of X–ray binary pulsars is usually well described by a hard power-law model with an exponential cut-off, sometimes with Fe K $\alpha$  emission lines. However, at low energies several sources show a significant excess over the main power-law, which has been described with different models (see La Palombara & Mereghetti 2006, for an overview). Although various physical processes have been invoked to produce it, its origin is still unclear. Hickox et al. (2004) showed that the origin of the *soft excess* is related to the source total luminosity and that a spectral component of this type has been detected in all the X–ray pulsars with a sufficiently high flux and small absorption. In fact, most of the soft excess sources are at small distances and/or away from the Galactic plane. This suggests that the presence of a soft spectral component could be a very common, if not an ubiquitous, feature intrinsic to X–ray pulsars. Since the study of the soft part of the spectrum in Galactic sources is affected by the interstellar ab-

sorption present in the Galactic plane, the best sources to study this feature are the transient pulsars in the Magellanic Clouds (MCs). They can reach high luminosities ( $L_X > 10^{38}$  erg s<sup>−1</sup>), are at well known distances, and, thanks to the low absorption in the MCs direction, can provide high-statistics spectra at low energies. In particular, the Small Magellanic Cloud (SMC) hosts more than 100 Be/X–ray Binary systems, about 70 of which show periodic pulsations (see, e.g. Haberl et al. 2012; Sturm et al. 2013; Klus et al. 2014).

One of the most interesting pulsars in the SMC is RX J0059.2–7138, also known as SXP 2.76, which was discovered in 1993 by *ROSAT* (Hughes 1994). A Be type star was found in its error region and proposed as a candidate counterpart (Southwell & Charles 1996). Optical photometry of this star revealed a periodicity of 82 days, likely related to the orbital period of the system (Schmidtke et al. 2006, Bird et al. 2012). The *ROSAT* X–ray spectrum of RX J0059.2–7138 was unusually soft, consisting of a low temperature black-body component ( $kT = 35$  eV) plus a steep power-law (photon index  $\Gamma = 2.4$ ). The presence of a soft excess was confirmed by a simultaneous *ASCA* observation, which also

\* E-mail: sidoli@iasf-milano.inaf.it

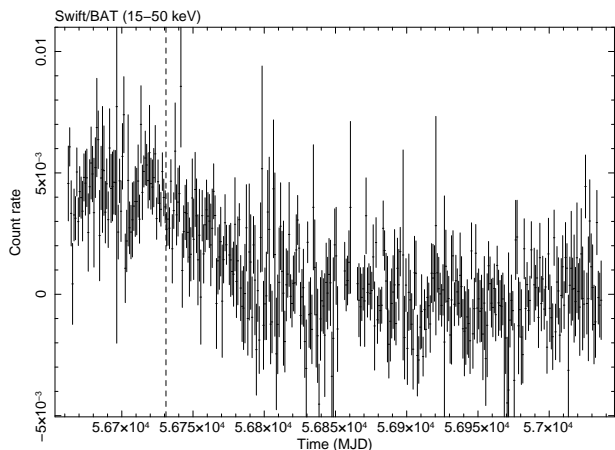


**Figure 1.** RX J0059.2–7138 outburst as observed by *Swift*/BAT (15–50 keV). The bin time is one day. The BAT light curve is publicly available at [HTTP://SWIFT.GSFC.NASA.GOV/RESULTS/TRANSIENTS/](http://swift.gsfc.nasa.gov/results/transients/) (Krimm et al. 2013). The date of our *XMM-Newton* observation is indicated by the vertical dashed line.

detected X-ray pulsations with a period of 2.76 s (Kohno et al. 2000). The simultaneous analysis of the *ROSAT* and *ASCA* data showed that the soft component could be described with either emission from a thin thermal plasma ( $kT=0.37$  keV) or a broken power-law, while a hard power-law ( $\Gamma=0.43$ ) described well the spectrum above 2 keV. Both components had a phase-averaged luminosity of  $\sim 10^{38}$  erg s $^{-1}$  (0.1–10 keV): the hard component dominated above 2 keV and showed sinusoidal pulsations with a pulsed fraction of  $\sim 37\%$ , while no pulsations were detected in the soft component, which dominated below 1 keV (Kohno et al. 2000).

After the 1993 observations, no other bright outbursts were seen from RX J0059.2–7138 until 2013, except for two detections of the source with PCA *RXT-E* in September 2002 and in November 2004 reported by Galache et al. (2008). The 2013 outburst was discovered with the *Swift*/BAT instrument, which detected the source starting from December 26 (see Fig. 1; Krimm et al. 2014). A couple of weeks later, *INTEGRAL* monitoring observations of the SMC confirmed the bright status of the source (Coe et al. 2014). After the discovery of this outburst, we triggered our *XMM-Newton* Target of Opportunity program aimed at investigating the soft excess in high luminosity Be/X-ray transients (hereafter Be/XRTs) thus obtaining an observation of RX J0059.2–7138 in March 2014. Here we report the results of this observation.

## 2 OBSERVATIONS AND DATA REDUCTION

RX J0059.2–7138 was observed by *XMM-Newton* between 2014 March 14 and 15, for a net exposure of  $\sim 19$  ks (see Table 1 for the observation log). In Fig. 1 we show the time of the *XMM-Newton* observation in the context of the outburst as observed by *Swift*/BAT (15–50 keV).

The *XMM-Newton* Observatory carries three 1500 cm $^2$  X-ray telescopes, each with an European Photon Imaging Camera (EPIC; 0.2–12 keV) at the focus. Two of the EPIC detectors use MOS CCDs (Turner et al. 2001) and one uses pn CCDs (Strüder et al. 2001). Reflection Grating Spectrometer (RGS; 0.4–2.1 keV) arrays (den Herder et al. 2001) are located in the telescopes with MOS cameras at their primary focus. The EPIC cam-

eras were operated in different modes, but always adopting the thin 1 filter: pn in Small Window, MOS1 in Imaging Prime Partial Window2 (small window), MOS2 in Timing Fast Uncompressed in the central CCD, while in Imaging Mode in the other CCDs. The time resolution is 5.7 ms, 0.3 s and 1.75 ms in the pn, MOS1 and MOS2, respectively. The data were reprocessed using version 13.5 of the Science Analysis Software (SAS) with standard procedures.

The RGSs were operated in spectroscopy mode and their data were analysed in the energy range 0.4–2.1 keV. The SAS task RGSPROC was used to extract the RGS1 and RGS2 spectra, which were later combined into one single grating spectrum using RGS COMBINE.

EPIC source counts were extracted from circular regions of 40'' radius for both the pn and MOS1, adopting PATTERN from 0 to 4 (mono- and bi-pixel events) in the pn and from 0 to 12 (up to 4-pixel events) in the MOS1. Background counts were obtained from similar sized regions offset from the source positions. Due to calibration issues in the MOS2 data (see Appendix A for details), we decided to use only the pn and MOS1 data for the spectral analysis, while we used all three EPIC data sets for the timing analysis. No further filtering based on the background level was necessary. Appropriate response matrices were generated using the SAS tasks ARFGEN and RMFGEN.

Free relative normalizations between the two cameras were included to account for uncertainties in instrumental responses. The normalization factor for the MOS1 spectra relative to PN (factor fixed at 1) was always around  $0.965 \pm 0.007$ . All spectral uncertainties and upper-limits are given at 90% confidence level for one interesting parameter.

In the spectral fitting we adopted the interstellar abundances of Wilms et al. (2000) and photoelectric absorption cross-sections of Balucinska-Church & McCammon (1992), using the absorption model PHABS in XSPEC. We checked that using a different absorption model (TBABS in XSPEC) with Wilms et al. (2000) abundances and cross sections by Verner et al. (1996) similar spectral fit results were obtained.

## 3 ANALYSIS AND RESULTS

### 3.1 Timing Analysis

The data from the three EPIC cameras in the 0.15–12 keV range were used for the timing analysis after conversion of their times of arrival to the Solar System barycenter. Using the  $Z_2^2$  test, the spin period of RX J0059.2–7138 was measured to be  $P_{\text{spin}} = 2.762383(5)$  s.

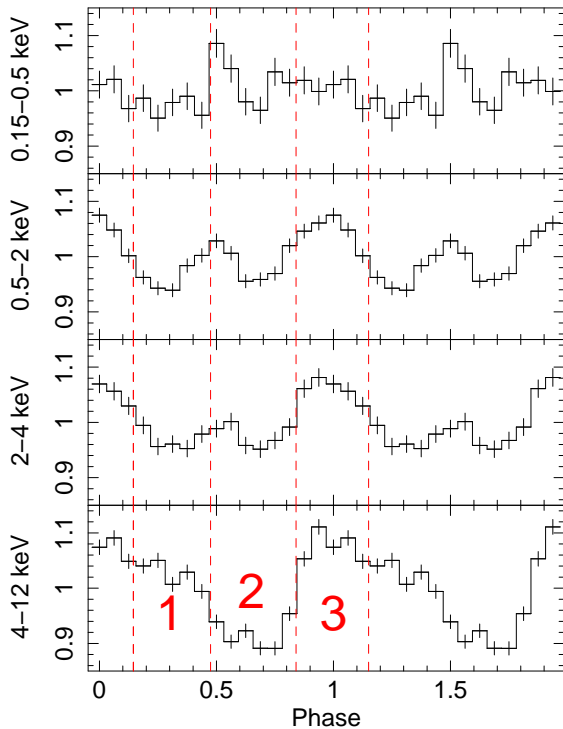
Following Kohno et al. (2000), we defined the pulsed fraction as  $(I_{\text{max}} - I_{\text{min}})/2I_{\text{average}}$ , where  $I_{\text{max}}$ ,  $I_{\text{min}}$ , and  $I_{\text{average}}$  are the maximum, minimum, and average count rate, respectively. The average pulsed fraction in the 2–10 keV energy range was  $8.9 \pm 0.5\%$  and during the observation the value did not change more than  $\sim 20\%$ .

With respect to the last observation performed in 1993 (MJD 49119–49120) with *ASCA*, when Kohno et al. (2000) found  $P_{\text{spin}} = 2.763221(4)$  s, our value implies an average spin-up rate of  $\dot{P}_{\text{spin}} = -(1.27 \pm 0.01) \times 10^{-12}$  s s $^{-1}$ .

In Fig. 2 we show the EPIC pn pulse profiles in different energy ranges. The pulse shape is clearly energy-dependent, with a broader single asymmetric peak in the 4–12 keV range, whereas a clear secondary pulse emerges at intermediate energies (0.5–4 keV). Below 0.5 keV the pulsations are less evident, but still significant (at  $3.6 \sigma$  confidence level). The pulse profile evolution with

**Table 1.** Summary of the *XMM-Newton* observation (ID. 0674730201) of RX J0059.2–7138

| Instrument | Filter | Mode         | Start and End Times |                     | Net Exp. time (ks) | Net count rate (s <sup>-1</sup> ) |
|------------|--------|--------------|---------------------|---------------------|--------------------|-----------------------------------|
| pn         | Thin 1 | Small Window | 2014-03-14 19:45:57 | 2014-03-15 01:10:34 | 13.7               | 19.24±0.04                        |
| MOS1       | Thin 1 | Small Window | 2014-03-14 19:40:09 | 2014-03-15 01:07:44 | 19.6               | 5.92±0.02                         |
| MOS2       | Thin 1 | Timing       | 2014-03-14 19:40:48 | 2014-03-15 01:03:30 | 19.4               | 5.86±0.02                         |
| RGS1       | –      | Specroscopy  | 2014-03-14 19:39:58 | 2014-03-15 01:11:55 | 19.9               | 0.246±0.004                       |
| RGS2       | –      | Specroscopy  | 2014-03-14 19:40:06 | 2014-03-15 01:11:53 | 19.8               | 0.299±0.004                       |


**Figure 2.** RX J0059.2–7138 pulse profiles observed with the EPIC pn camera in four energy bands. The vertical dashed lines and the numbers mark the three spin-phase intervals adopted for the phase-selected spectroscopy (Sect. 3.2.2).

energy is clearly shown also by the phase-energy image (Fig. 3). This image represents the number of source counts in small phase and energy intervals, normalized with respect to the phase-averaged spectrum (see Tiengo et al. 2013). A deficit of counts (marked by the white box) over a narrow range of energies ( $\sim 7$ –8 keV) in the phase interval  $\Delta\phi=0.7$ –0.8 is evident. This possible evidence for a phase-dependent absorption line will be discussed in Sect. 3.2.

## 3.2 EPIC Spectroscopy

### 3.2.1 Time-averaged spectrum

We searched for possible spectral variability within the *XMM-Newton* exposure, by extracting light curves in different energy ranges. We found no strong evidence for intensity and spectral variability on timescales longer than the spin periodicity, so we ex-

**Table 2.** Results of the simultaneous EPIC pn and MOS1 fit of the time-averaged spectrum (0.2–12 keV). The double-component continuum consists of a cut-off power law (CUTOFFPL in XSPEC) and a black-body model. Both components are equally absorbed with column density  $N_{\text{H}}$ . Three Gaussian lines in emission are needed to account for positive residuals in the spectrum (the line at  $E_{\text{line}1}$  has been added only in the pn spectrum, being of instrumental origin). The parameters of the black-body component are its temperature,  $kT_{\text{bb}}$ , and its radius,  $r_{\text{bb}}$ . A distance of 61 kpc is assumed (Hilditch et al. 2005). The cut-off power-law continuum is defined as  $A(E)=kE^{-\Gamma} \exp -(E/E_c)$ , where  $\Gamma$  is the photon index and  $E_c$  is the e-folding energy of the exponential rolloff (in units of keV).  $\text{Flux}_{\text{line}\#N}$  is the total flux in the Gaussian line  $\#N$ .  $\text{EW}_{\text{line}\#N}$  is the equivalent width of the line  $\#N$  (eV). The unabsorbed flux is in units of  $\text{erg cm}^{-2} \text{ s}^{-1}$ , the luminosity in units of  $\text{erg s}^{-1}$ .  $L_{\text{bb}}/L_{\text{cpl}}$  is the fraction of X-ray emission (corrected for the absorption) contributed by the soft component with respect to the cut-off power-law, in the broad energy band 0.01–10 keV.

| Parameter   | Value                         |
|---|-------------------------------|
| $N_{\text{H}}$ ( $10^{20} \text{ cm}^{-2}$ )                        | $2.3^{+0.6}_{-0.5}$           |
| $kT_{\text{bb}}$ (keV)  | $0.093^{+0.005}_{-0.005}$     |
| $r_{\text{bb}}$ (km)  | $350^{+80}_{-50}$             |
| $\Gamma$  | $0.44^{+0.02}_{-0.02}$        |
| $E_c$ (keV)   | $36^{+8}_{-6}$                |
| $E_{\text{line}1}$ (keV)  | $2.23 \pm 0.01$               |
| $E_{\text{line}2}$ (keV)  | $6.58^{+0.07}_{-0.06}$        |
| $\sigma_{\text{line}2}$ (keV)                                       | $0.13^{+0.09}_{-0.08}$        |
| $\text{Flux}_{\text{line}2}$ ( $\text{ph cm}^{-2} \text{ s}^{-1}$ ) | $(6 \pm 2) \times 10^{-5}$    |
| $\text{EW}_{\text{line}2}$ (eV)                                     | $30 \pm 10$                   |
| $E_{\text{line}3}$ (keV)  | $0.96^{+0.02}_{-0.03}$        |
| $\sigma_{\text{line}3}$ (keV)                                       | $0.095^{+0.030}_{-0.024}$     |
| $\text{Flux}_{\text{line}3}$ ( $\text{ph cm}^{-2} \text{ s}^{-1}$ ) | $15^{+5}_{-4} \times 10^{-5}$ |
| $\text{EW}_{\text{line}3}$ (eV)                                     | $30 \pm 8$                    |
| $L_{\text{bb}}/L_{\text{cpl}}$ (0.01–10 keV)                        | 1.7%                          |
| Unabsorbed flux (0.5–10 keV)  | $1.58 \times 10^{-10}$        |
| Luminosity (0.5–10 keV)   | $7 \times 10^{37}$            |
| $\chi^2_{\nu}/\text{dof}$   | 1.405/546                     |

tracted a time-averaged spectrum for the whole pn and MOS1 exposures.

The main spectral structures in addition to a simple absorbed power-law component, can be seen in Fig. 4 (*upper panel*): 1)–a soft excess below  $\sim 0.5$  keV; 2)–a high energy cut-off; 3)–a narrow feature at 2.2 keV (present only in the pn data, very likely due to residual calibration uncertainties around the Au edge); as done by other authors (e.g. Díaz Trigo et al. 2014) we model it with a Gaus-

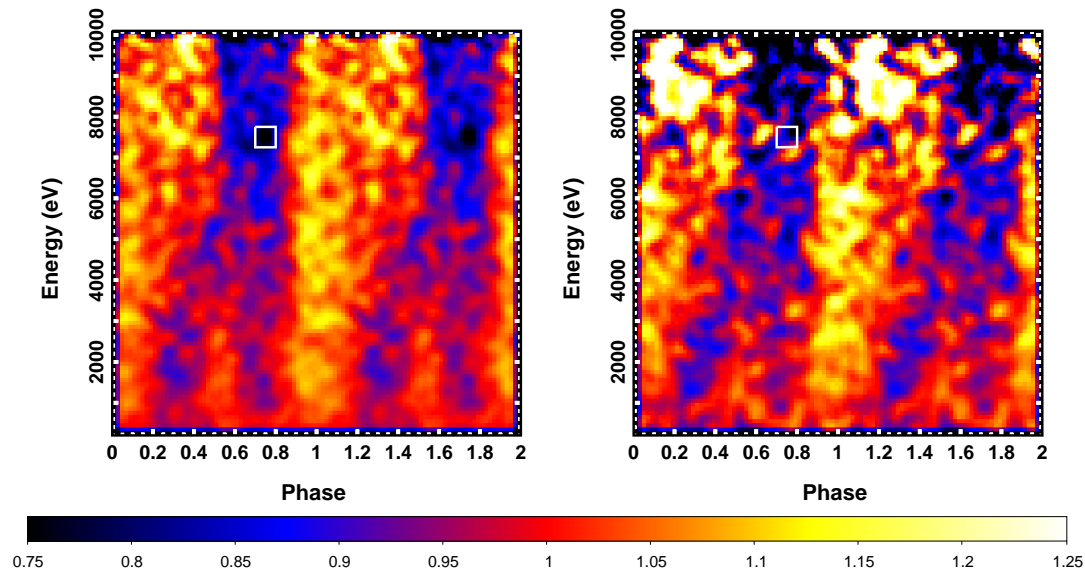


**Figure 3.** RX J0059.2–7138 phase-energy image (normalized to the phase-averaged spectrum) obtained from the EPIC pn and MOS2 data (the MOS1 time resolution is too poor for such a fine phase binning). The small white box marks a *hole* in the image, indicating a deficit of counts, with respect to the average spectrum, in a narrow range of energies ( $\sim 7$ -8 keV) and spin phases ( $\Delta\phi=0.7$ -0.8).

sian line, but we will not discuss it further; 4)-an emission line at 6.5-6.8 keV; 5)-a broad positive residual around 0.9-1.0 keV. The presence of the latter structure also in the RGS spectrum (see below, Sect. 3.3), excludes a calibration/instrumental origin, thus we decided to include an additional broad Gaussian line to fit it.

To account for these structures, we adopted a double-component continuum consisting of a cut-off power-law plus a black-body model together with the three Gaussian lines. The results are reported in Table 2 and displayed in Fig. 4 (*lower panel*).

We also tried a hot thermal plasma model (MEKAL in XSPEC) instead of the black-body to fit the soft excess, with similar  $\chi^2$  results: all the parameters were consistent with those reported in Table 2, except for the column density  $N_{\text{H}}=(4.1 \pm 0.6) \times 10^{20} \text{ cm}^{-2}$  and the fraction of X-ray emission contributed by the soft component with respect to the cut-off power-law, which was 7% (instead of 1.7%), in the energy band 0.01-10 keV. The parameters of the MEKAL model were the following: a plasma temperature  $kT_{\text{M}}=0.21 \pm 0.03$  keV, a very low metal abundance  $Z \lesssim 0.007 Z_{\odot}$  (too low for the SMC, see below), a normalization,  $norm_{\text{M}}$ , of  $0.025^{+0.008}_{-0.006} \text{ cm}^{-5}$  (in our case,  $norm_{\text{M}}=2.4 \times 10^{-62} \int n_e n_H dV$ , where  $n_e$  and  $n_H$  are the electron and hydrogen densities,  $V$  is the emitting volume).

We also tried to adopt two absorption models, one to account for the total Galactic absorption in the SMC direction ( $N_{\text{H}}$  fixed at  $6 \times 10^{20} \text{ cm}^{-2}$ ), the other one to account for the local absorption in the SMC (VPHABS model in XSPEC with an abundance fixed at 0.2 for metals, appropriate for the SMC), but we did not obtain better fits than using a single absorption model with a free column density. So, we decided to adopt a single model for the absorption (PHABS model in XSPEC). We also tried to fit the data with warm and ionized absorbers (like ABSORI in XSPEC; Done et al. 1992) in

addition to a neutral one accounting for the interstellar absorption, but this did not result in better fits.

### 3.2.2 Spin-phase-selected spectroscopy

Given the energy-dependence observed in the folded spin profiles (Figs. 2 and 3), it is not surprising that the fits to the time-averaged spectrum were not formally acceptable. To quantitatively explore the observed spectral evolution, we extracted three phase-selected spectra (marked by numbers in Fig. 2) for EPIC MOS1 and the pn:  $\Delta\phi=0.15$ -0.45 (spectrum n. 1),  $\Delta\phi=0.45$ -0.85 (spectrum n. 2),  $\Delta\phi=0.85$ -0.15 (spectrum n. 3).

The MOS1 and pn spectra were fitted simultaneously in the 0.2 to 12 keV range with the same model used for the time-averaged emission. Good fits were obtained with the spectral parameters listed in Table 3. Similar values were obtained using a MEKAL model instead of the black-body, but again with a very low metallicity ( $Z \lesssim 0.01 Z_{\odot}$ ).

The results reported in Table 3 indicate that the phase-dependent spectral variability is mainly due to variations in the high energy cut-off. The iron lines around  $\sim 6.6$  keV are significant at  $2.9 \sigma$ ,  $4.4 \sigma$  and  $4.1 \sigma$ , in spectra 1, 2 and 3, respectively. The significance was estimated by increasing the  $\Delta\chi^2$  value until the confidence region boundary of the Gaussian normalisation crosses 0. The iron line centroid energy shows variations from 6.77 keV (in spec. 1) to 6.54 keV (in spec. 2). In spec. 2 the centroid energy is compatible with transitions in Fe XXI-Fe XXII ions (Kallman & McCray 1982), in spec. 3 with Fe XXI-Fe XXV ions, while in spec. 1 (line centroid at 6.77 keV), it is not consistent (within the 90% errors) with any known line. Although the emission line in spec. 1 is significant at less than  $3 \sigma$ , if we identify it with emission from Fe XXV at 6.7 keV, a hint for a blue-shift

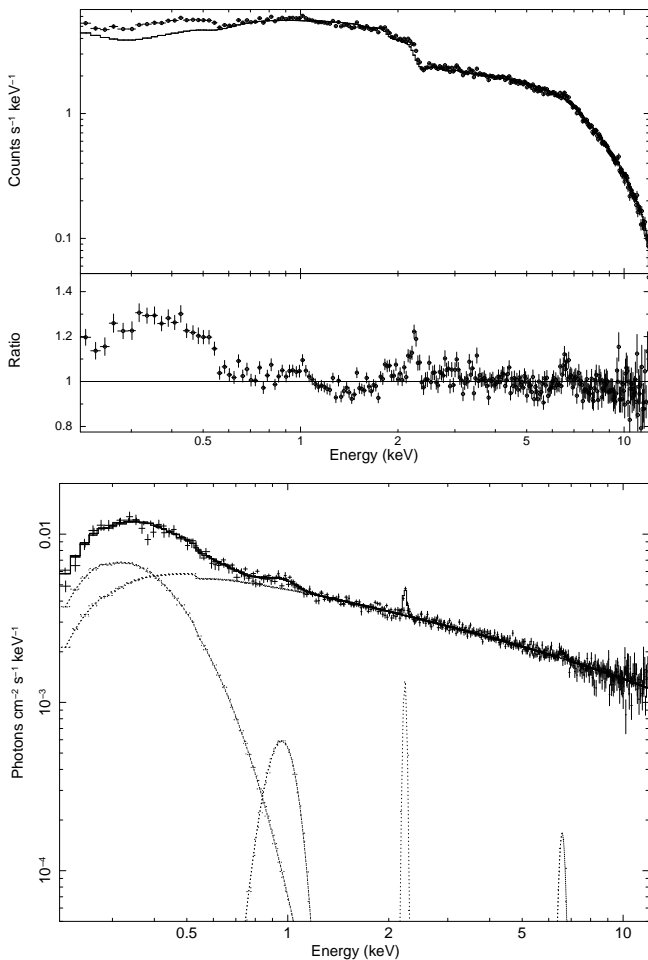


**Figure 4.** RX J0059.2–7138 EPIC time-averaged spectrum. *Upper panel* shows the fit of the pn data with a single power-law, to clearly show the main structures in the spectrum. *Lower panel* displays the photon spectrum from the EPIC pn and MOS1 observations fitted with the model reported in Table 2.

of  $900 \text{ km s}^{-1}$  is present, possibly indicating an outflowing photoionized plasma. Also the flux of the broad feature at 0.9–1 keV is variable along the spin profile, while the other spectral parameters are constant, within the uncertainties.

The phase-energy image (Fig. 3) shows a hint for a deficit of counts at  $\sim 7\text{--}8$  keV, with respect to the spin-averaged spectrum. This deficit, possibly indicating an absorption feature, occurs in a narrow range of spin phases ( $\phi \sim 0.7\text{--}0.8$ ). We extracted a spectrum corresponding to this phase interval and we fitted it adding a Gaussian line in absorption. The new fit gave a reduced  $\chi^2_{\nu} = 1.014$  for 464 dof (compared to  $\chi^2_{\nu} = 1.049$  for 467 dof with no line). The resulting line parameters were the following: centroid energy  $E_{\text{line4}} = 7.50 \pm 0.09$  keV, width  $\sigma_{\text{line4}} < 0.27$  keV, total  $\text{Flux}_{\text{line4}} = -(1.28^{+0.62}_{-0.79}) \times 10^{-4}$  photons  $\text{cm}^{-2} \text{ s}^{-1}$ , equivalent width  $\text{EW}_{\text{line4}} \sim -80$  eV. The single trial significance of this line is  $4.4 \sigma$ , but given that many phase intervals were explored, the overall significance is too small to claim a firm detection.

### 3.3 RGS Spectroscopy

The RGS first order spectra (0.4–2.1 keV) were extracted from the whole exposure and combined into a single grating spectrum. We fitted it with the same double-component model resulting from the time-averaged spectrum (black-body plus cut-off power-law). The inspection of the residuals clearly showed the presence of narrow lines (both in absorption and in emission), together with a broad structure around 0.9–1.0 keV (which was also clearly present in the EPIC spectra). The addition of Gaussian lines to account for them, resulted in the line parameters reported in Table 4. The spectrum is shown in Fig. 5. The two brightest narrow lines, at 0.5 and 0.65 keV, are firmly associated with N VII and O VIII Ly $\alpha$  lines, respectively, while the broad component at 0.92 keV is possibly due to different contributions: a blend of several emission lines from iron in a range of ionizations states, from Fe XVIII to Fe XX, a radiative recombination continuum (RRC) from O VIII, likely with superposed weak emission lines from ionized neon (Table 4). The parameters of this broad component observed in the RGS spectrum are consistent with what found with EPIC.

We then used a thermal plasma model (MEKAL) with free abundance instead of the black-body to account for the soft excess (with the metal abundance let free to vary, and resulting in a kT of  $\sim 0.23$  keV), but in this case only the narrow line at 0.65 keV could be well fitted. Also adopting additional MEKAL models with different temperatures or a CEMEKL model (a multi-temperature plasma emission model built from the mekal code, with emission measures following a power-law in temperature) we could not obtain acceptable fits to the other emission lines, likely indicative of a photoionized nature of the emitting matter. Two absorption lines were also found, with possible identifications listed in Table 4.

The O VII He $\alpha$  triplet is undetected, preventing us from using the so-called “G ratio” in He-like ions to obtain information on the ionization process and plasma density (Porquet & Dubau 2000). We could place the following upper limits (90% confidence level) to the fluxes of the three O VII triplet components:  $F < 3.1 \times 10^{-5}$  ph  $\text{cm}^{-2} \text{ s}^{-1}$  (forbidden line at 0.561 keV),  $F < 5.0 \times 10^{-5}$  ph  $\text{cm}^{-2} \text{ s}^{-1}$  (intercombination line at 0.569 keV),  $F < 3.4 \times 10^{-5}$  ph  $\text{cm}^{-2} \text{ s}^{-1}$  (resonance line at 0.574 keV).

## 4 DISCUSSION

The Be transient RX J0059.2–7138 in the SMC attracted attention because, like a few other X-ray pulsars, it showed a prominent soft excess, the origin of which is still uncertain (Hickox et al. 2004). Two were the main alternatives discussed by Hickox et al. to explain the soft excess in RX J0059.2–7138: either reprocessing of X-rays in the inner region of an accretion disc or optically thin, hot thermal emission.

Thanks to the large collecting area of *XMM-Newton*, the observation obtained during the recent new outburst of RX J0059.2–7138, allowed us to perform a more detailed study of this source, even if its luminosity of  $L_X = 7 \times 10^{37}$  erg  $\text{s}^{-1}$  (0.5–10 keV) was a factor  $\sim 3$  smaller than that observed in the 1993 *ROSAT* and *ASCA* data (Kohno et al. 2000).

The new period value,  $P_{\text{spin}} = 2.762383(5)$  s, implies an average spin-up rate of  $\dot{P}_{\text{spin}} = -(1.27 \pm 0.01) \times 10^{-12} \text{ s s}^{-1}$  in the  $\sim 20$  years between the two outbursts. This spin-up value is probably not representative of the true torques currently acting on the neutron star, since during the long time interval between the two outbursts, the pulsar could have been spinning-down, at least for

**Table 3.** Results of the spin-phase selected spectroscopy (spectra n. 1, 2 and 3 indicate spin phase intervals 0.15-0.45, 0.45-0.85, 0.85-0.15 respectively) fitting together the EPIC pn and MOS1 observations in the energy band (0.2–12 keV). The model is the same adopted in Table 2.

| Parameter   | 1                                 | 2                                    | 3                                    |
|---|-----------------------------------|--------------------------------------|--------------------------------------|
| $N_{\text{H}}$ ( $10^{20}$ cm $^{-2}$ )                 | $2.9^{+1.9}_{-1.3}$               | $2.1^{+0.9}_{-0.8}$                  | $1.9^{+1.2}_{-1.0}$                  |
| $kT_{\text{bb}}$ (keV)                                  | $0.09^{+0.01}_{-0.02}$            | $0.099^{+0.008}_{-0.007}$            | $0.09^{+0.01}_{-0.01}$               |
| $r_{\text{bb}}$ (km)                                    | $420^{+700}_{-130}$               | $300^{+100}_{-60}$                   | $350^{+230}_{-90}$                   |
| $\Gamma$  | $0.43^{+0.04}_{-0.05}$            | $0.42^{+0.03}_{-0.03}$               | $0.37^{+0.04}_{-0.04}$               |
| $E_c$ (keV)   | $>45$                             | $20^{+4}_{-3}$                       | $22^{+5}_{-4}$                       |
| $E_{\text{line1}}$ (keV)                                | $2.23^{+0.03}_{-0.03}$            | $2.23^{+0.02}_{-0.02}$               | $2.25^{+0.03}_{-0.03}$               |
| $E_{\text{line2}}$ (keV)                                | $6.77^{+0.06}_{-0.04}$            | $6.54^{+0.05}_{-0.04}$               | $6.59^{+0.08}_{-0.08}$               |
| $\sigma_{\text{line2}}$ (keV)                           | $<1.6$                            | $<0.09$                              | $0.12^{+0.09}_{-0.08}$               |
| $\text{Flux}_{\text{line2}}$ (ph cm $^{-2}$ s $^{-1}$ ) | $(4.3 \pm 2.4) \times 10^{-5}$    | $(4.9^{+2.7}_{-1.8}) \times 10^{-5}$ | $(8.4^{+3.9}_{-3.6}) \times 10^{-5}$ |
| $\text{EW}_{\text{line2}}$ (eV)                         | $23 \pm 13$                       | $30^{+16}_{-10}$                     | $43^{+20}_{-18}$                     |
| $E_{\text{line3}}$ (keV)                                | $0.92^{+0.07}_{-0.17}$            | $0.99^{+0.03}_{-0.04}$               | $0.93^{+0.05}_{-0.05}$               |
| $\sigma_{\text{line3}}$ (keV)                           | $0.19^{+0.09}_{-0.06}$            | $<0.09$                              | $0.10^{+0.06}_{-0.04}$               |
| $\text{Flux}_{\text{line3}}$ (ph cm $^{-2}$ s $^{-1}$ ) | $(40^{+50}_{-20}) \times 10^{-5}$ | $(9^{+5}_{-4}) \times 10^{-5}$       | $(16^{+14}_{-7}) \times 10^{-5}$     |
| $\text{EW}_{\text{line3}}$ (eV)                         | $80^{+80}_{-30}$                  | $18^{+11}_{-8}$                      | $31^{+23}_{-14}$                     |
| $L_{\text{bb}}/L_{\text{cpl}}$ (0.01-10 keV)            | 0.02                              | 0.017                                | 0.015                                |
| Unabsorbed flux (0.5-10 keV)                            | $1.6 \times 10^{-10}$             | $1.4 \times 10^{-10}$                | $1.7 \times 10^{-10}$                |
| $\chi^2_{\nu}/\text{dof}$                               | 1.041/517                         | 1.067/522                            | 1.033/518                            |

**Table 4.** Main lines identified in the RX J0059.2–7138 RGS spectrum (0.4–2.1 keV). Negative fluxes and negative equivalent widths (EWs) mean that the Gaussian lines are in absorption.

| Energy <sub>observed</sub><br>(keV) | Ion  | $\lambda_{\text{lab}}$<br>(Å) | Energy <sub>lab</sub><br>(keV) | $\sigma$<br>(eV)    | Flux<br>( $10^{-5}$ ph cm $^{-2}$ s $^{-1}$ ) | EW<br>(eV)       |
|-------------------------------------|--|-------------------------------|--------------------------------|---------------------|---|------------------|
| $0.500^{+0.001}_{-0.002}$           | N VII  | 24.779 (Ly $\alpha$ )         | 0.50                           | $2.4^{+2.0}_{-1.0}$ | $6.8 \pm 2.7$                                 | $7 \pm 3$        |
| $0.6516^{+0.0026}_{-0.0016}$        | O VIII   | 18.967 (Ly $\alpha$ )         | 0.65                           | $4^{+2}_{-1}$       | $5.7 \pm 2.0$                                 | $9 \pm 3$        |
| $0.811^{+0.003}_{-0.007}$           | Fe XVII (?)  | 15.2610                       | 0.81                           | $5^{+7}_{-2}$       | $-2.8^{+1.2}_{-1.5}$                          | $-5 \pm 2$       |
| $0.921^{+0.026}_{-0.024}$           | Fe XVIII-Fe XX (blended?)<br>or RRC from O VIII (?)– Ne IX (?) | —<br>13.45                    | —<br>0.89; 0.91                | $60^{+30}_{-40}$    | $17^{+5}_{-6}$                                | $34^{+20}_{-14}$ |
| $1.0795^{+0.0009}_{-0.0056}$        | Fe XXII (?)  | 11.490                        | 1.079                          | $<9$                | $4.7^{+2.6}_{-2.4}$                           | $11 \pm 6$       |
| $1.114^{+0.013}_{-0.012}$           | Fe XXIII (?)   | 11.019                        | 1.125                          | $9^{+21}_{-6}$      | $-4.4^{+1.9}_{-2.8}$                          | $-9^{+4}_{-5}$   |

part of the time. With the reasonable assumption that an accretion disk is present during the observed outburst, we can discuss the results in the framework of the Ghosh & Lamb (1979) theory of accretion torques. For a given neutron star mass, radius, and dipolar magnetic field, the spin period derivative,  $\dot{P}$ , is expected to scale as  $PL^{3/7}$  (where  $P$  is the spin period,  $L$  is the X-ray luminosity). Assuming  $M = 1.4 M_{\odot}$ ,  $R = 10$  km,  $L = 10^{38}$  erg s $^{-1}$ ,  $B = 10^{12}$  G the expected spin-up rate for RX J0059.2–7138 during the *XMM-Newton* observation is  $\dot{P} \sim -6.8 \times 10^{-11}$  s s $^{-1}$  (eq. 15 in Ghosh & Lamb 1979). As expected, this value is larger (by a factor of  $\sim 50$ ) than the time averaged spin-up rate between 1993 and 2014.

Although the pulsed fraction observed in 2013 ( $8.9 \pm 0.5$  %) was smaller than in 1993 (37%), the large number of counts col-

lected by the three EPIC cameras allowed us to see interesting variations of the pulse profile as a function of energy that were not evident in the previous observations. The pulse profile is double-peaked at intermediate energies (0.5–4 keV) and for the first time pulsations were seen also below 0.5 keV. In principle, the presence of pulsations in the soft energy range might give some information on the origin of the soft excess (see below), but in practice this is complicated by the fact that both the soft excess and the hard power law contribute to the counts in this energy range and could be responsible for the observed modulation.

Our observation confirms the presence of a soft excess in RX J0059.2–7138. Its 0.2–12 keV spectrum could be well fitted by a double-component continuum with a hard cut-off power-law ( $\Gamma \sim 0.44$ ) together with a soft excess equally well modelled by

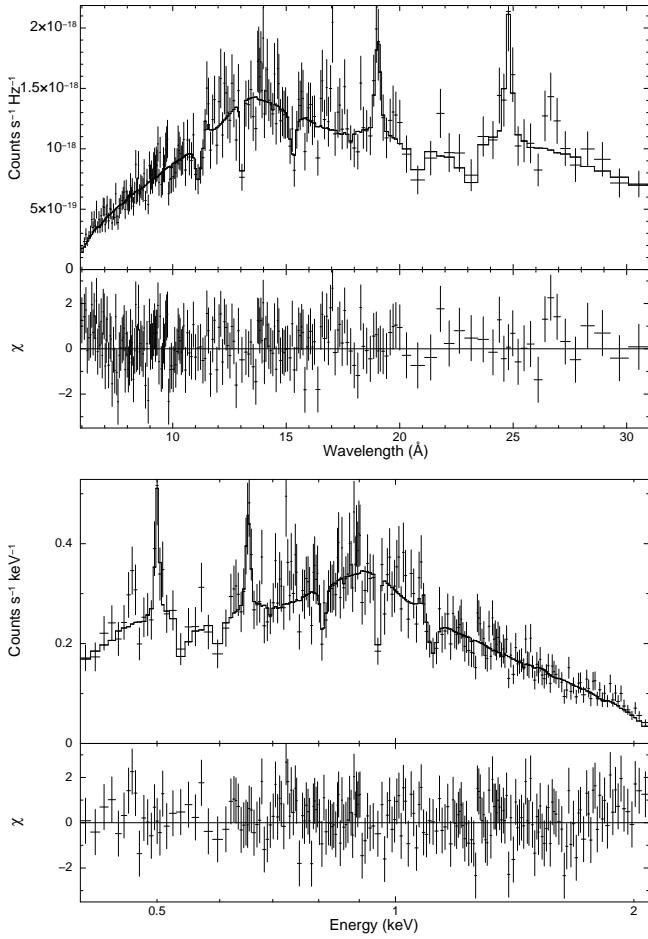


**Figure 5.** Results of the RGS spectroscopy. The counts spectrum is shown when fitting the combined RGS1 and RGS2 spectra with a double component continuum (a black-body together with a power-law) modified by the absorption, including six Gaussian lines to account for the brightest lines (four in emission and two in absorption; see Table 4). In the *upper panel* the spectrum is in units of wavelength, while in the *lower panel* it is in units of energy. Spectra have been severely rebinned in these plots, to better show the residuals.

either a soft black-body ( $kT \sim 0.1$  keV), or a hot thermal plasma model ( $kT \sim 0.2$  keV). While these spectral parameters are similar to what found in 1993, the relative contribution of the soft component to the total luminosity was much lower in 2014: the 0.1–10 keV luminosities of the soft and hard spectral components were  $L_{bb} = 10^{36}$  erg s $^{-1}$  and  $L_{ep1} = 7.1 \times 10^{37}$  erg s $^{-1}$  in 2014, while they were  $L_{soft} = 8 \times 10^{37}$  erg s $^{-1}$  and  $L_{hard} = 1.8 \times 10^{38}$  erg s $^{-1}$  in 1993, implying a soft to hard luminosity ratio of 1.5% (in 2014) instead of 44% (in 1993).

We discovered several features in the RX J0059.2–7138 spectrum: narrow lines from ionized oxygen and nitrogen (in the RGS data), a broad feature at 0.9–1 keV, likely produced by Fe-L shell emission (both in the RGS and EPIC data), and an iron emission line at  $\sim 6.6$  keV. The latter is clearly evident in the time-averaged spectrum. There is some evidence that its centroid energy varies as a function of the pulsar spin phase, but the significance of the line is marginal ( $< 3\sigma$ ) when it attains the highest energy.

We detected a phase dependence of the cut-off energy (from  $E_c \sim 20$  keV to  $E_c > 45$  keV), which is the main responsible for the

spectral variability with the spin phase. A similar behavior of high-energy cut-off is unusual in X-ray pulsars (an example is the low-mass X-ray binary pulsar 4U 1626-67, Coburn et al. 2002). We observed also a phase dependence of the flux contributed by the broad emission component at 0.9–1 keV, that can be explained by a variable emitting area illuminated/photoionized by the pulsar beam.

An accretion disc is a natural reprocessing site for the X-ray emission emitted from the accreting pulsar, especially when its luminosity is high ( $\sim 10^{38}$  erg s $^{-1}$ ) and photons preferentially escape in a fan-beam from the accretion column (e.g. Parmar et al. 1989), favouring an X-ray illumination of the equatorial regions. Following Hickox et al. 2004, we can assume that black-body emission with luminosity  $L_{SOFT} = \Omega L_X$  (where  $L_X$  is the total X-ray luminosity) results from reprocessing by optically thick material located at a distance  $R$  and subtending a solid angle  $\Omega$  with respect to the central X-ray source. Independent on the exact geometry of the reprocessing region, the distance  $R$  can be estimated from the relation

$$R^2 = \frac{L_X}{4\pi\sigma T_{BB}^4}$$

(note that this is different from the radius ( $r_{bb}$ ) resulting from the normalization of the black-body component in the spectral fit (Tables 2 and 3)). If the reprocessing region is a shell at the inner edge of the disc,  $R$  should be of the order of the magnetospheric radius,  $R_m$  (or of the corotation radius if the pulsar is rotating close to the equilibrium period). Adopting the RX J0059.2–7138 phase-averaged luminosity  $L_X = 7 \times 10^{37}$  erg s $^{-1}$  (0.5–10 keV) and the black-body temperature,  $T_{BB}$ , of 0.09 keV (Table 2), we obtain a distance  $R = 3 \times 10^8$  cm, which is indeed very similar to the corotation radius  $R_{cor} = 3.3 \times 10^8$  cm. An estimate of the magnetospheric radius (Davies & Pringle 1981) can be obtained from the relation

$$R_m \sim 1.5 \times 10^8 m_1^{1/7} R_6^{10/7} L_{37}^{-2/7} B_{12}^{4/7} \text{ cm},$$

where  $m_1$  is the neutron star (NS) mass in units of solar masses,  $R_6$  is the NS radius in units of  $10^6$  cm,  $L_{37}$  is the X-ray luminosity in units of  $10^{37}$  erg s $^{-1}$ ,  $B_{12}$  is the NS magnetic field in units  $10^{12}$  Gauss. If for RX J0059.2–7138 we assume  $B_{12} = 1$  we obtain  $R_m \sim 10^8$  cm. If the soft excess is caused by reprocessing of the X-ray pulsar emission by the inner edge of the accretion disc, some pulsations in the soft part of the spectrum are expected, as indeed it was found. In this scenario, the narrow lines we discovered at low energies in the RGS spectrum and the ionized iron line at 6.6 keV can be produced by a plasma located in the disc atmosphere. They require the presence of matter with very different ionizations stages. Indeed, while plasma with highly ionized oxygen and nitrogen is characterized by a ionization parameter  $\xi \sim 100$  erg cm s $^{-1}$  ( $\xi = L/nR^2$ , where  $L$  is the luminosity of the ionizing source,  $n$  is the plasma density,  $R$  is the distance of the photoionized matter from the ionizing source), the presence of highly ionized iron Fe XXV implies  $\xi = 1000$  erg cm s $^{-1}$  (Kallman & McCray 1982). The widths we derived for the N VII and O VIII Ly $\alpha$  lines are larger than the RGS energy resolution and imply velocities of  $\sim 1,000$ – $2,500$  km s $^{-1}$  for the emitting plasma, as expected for matter rotating at distances of a few  $\times 10^9$  cm from the neutron star. Given the high X-ray luminosity, the presence of the accretion disc, and the detection of narrow lines from matter with very different ionization stages not compatible with a single plasma temperature, we can interpret the soft excess as the result of reprocessing from the inner edge of the disc and the narrow lines as due to photoionized plasma in regions above the disc.

An alternative interpretation is that the soft excess in RXJ0059.2–7138 is entirely emitted by a thermal hot plasma (Hickox et al. 2004). Using a MEKAL model to fit the RGS spectrum, we could account well *only* for the O VIII Ly $\alpha$  emission line, which we interpret as a further indication of the presence of photoionization, and obtained a metal abundance ( $Z \lesssim 0.01 Z_{\odot}$ ) too low for the SMC. The emission measure obtained from the normalization of the MEKAL model is  $n^2V \sim 10^{60} \text{ cm}^{-3}$ . Since the gas density in this case should be  $n < 10^{12} \text{ cm}^{-3}$ , the emitting spherical region for the optically thin plasma should have a radius  $R_{\text{cloud}} > 6 \times 10^{11} \text{ cm}$ , and no pulsations in the soft excess are expected.

Kohno et al. (2000) found wavy structures below 1 keV in their *ROSAT* plus *ASCA* spectrum and explained them with the presence of a deep edge-like structure at 0.5 keV, caused by an over-abundance of neutral oxygen (about 6 times solar) in the circumstellar matter. However, this was at odds with the very low metal abundance (0.02 solar) in their best-fit thermal plasma model. These authors concluded that the oxygen over-abundance is real, while the MEKAL model is un-physical. Also our *XMM-Newton* spectrum showed wavy structures below 1 keV, which we fitted with a broad Gaussian line at  $\sim 0.96 \text{ keV}$ , but we found no evidence for a neutral oxygen edge at 0.54 keV deeper than the one ascribable to the best-fitting  $N_{\text{H}}$ . We note that acceptable fits to the EPIC spin-phase selected spectra adopting a single absorption model with variable metal abundances (VPHABS in XSPEC) could be obtained *only* deleting the Gaussian component at 0.96 keV. However, in this case, an oxygen overabundance around 30 times solar was obtained, which we think is unlikely. Moreover, the resulting column density was very low ( $\sim 5 \times 10^{19} \text{ cm}^{-2}$ ), one order of magnitude lower than the Galactic one. If, instead, we use two absorption models, one for the Galactic absorption (PHABS) and one with variable abundances for the SMC absorption (VPHABS), the column density of the latter becomes compatible with zero and the fit is insensitive to the metal abundances. Given that the neutral oxygen edge falls within two bright emission lines in the RGS spectrum (N VII and O VIII), we believe that the edge-like structure at 0.5 keV observed by Kohno et al. (2000) was due to the low spectral resolution of the *ROSAT* plus *ASCA* spectra and to the presence of the nearby emission component at 0.9–1 keV.

A hint of an absorption line at 7.5 keV was present only in a narrow range of spin phases ( $\Delta\phi=0.7\text{--}0.8$ ). Since its energy is not consistent with any known line feature (except for the  $K_{\alpha}$  line from neutral Ni at 7.48 keV, which we consider very unlikely, given the highly ionizing flux from the X-ray pulsar), it is tempting to associate it with a cyclotron resonant scattering feature. In this case, its energy would imply a magnetic field in the scattering region of  $6.5 \times (1+z) \times 10^{11} \text{ G}$ , where  $z$  is the gravitational redshift.

## 5 CONCLUSIONS

The main results of our *XMM-Newton* observation obtained during the second bright outburst from the SMC Be/XRT RXJ0059.2–7138 can be summarized as follows :

- The continuum X-ray spectrum is complex and requires several components: a hard power law with a phase-dependent high-energy cut-off, a soft excess below 0.5 keV well fit by a black-body model, and a broad emission feature at  $\sim 0.9\text{--}1 \text{ keV}$ .
- We discovered narrow emission and absorption lines from oxygen, nitrogen and iron in different ionization stages.

- The relative contribution of the soft excess component to the total luminosity was smaller than in the 1993 observations (1.5% wrt 44%), when the source was a factor  $\sim 3$  brighter.

- Contrary to what observed in 1993, the pulsar pulse profile was strongly energy-dependent and pulsations were detected also below 0.5 keV. The pulsar spin period of  $P_{\text{spin}}=2.762383(5) \text{ s}$  implies an average spin-up rate of  $\dot{P}_{\text{spin}} = -(1.27 \pm 0.01) \times 10^{-12} \text{ s s}^{-1}$  in the  $\sim 20$  years elapsed after the only other period measurement of this source.

These findings lead us to interpret the soft X-ray excess in this source as due to reprocessing of the pulsar emission from (part of) the inner edge of the accretion disc at a radius of  $\sim 3 \times 10^8 \text{ cm}$ . The disc inner boundary is consistent with a magnetic field of the order of  $10^{12} \text{ G}$  which could also explain the possible absorption feature at 7.5 keV as an electron cyclotron line. The observed narrow lines are most likely produced by photoionization of plasma located above the inner regions of the accretion disc.

## ACKNOWLEDGMENTS

This work is based on data from observations with *XMM-Newton*. *XMM-Newton* is an ESA science mission with instruments and contributions directly funded by ESA Member States and the USA (NASA). LS thanks A. Pollock and A. Giménez-García for interesting discussions. PE acknowledges a Fulbright Research Scholar grant administered by the U.S.–Italy Fulbright Commission and is grateful to the Harvard–Smithsonian Center for Astrophysics for hosting him during his Fulbright exchange. We acknowledge financial contribution from the agreement ASI-INAF I/037/12/0.

## APPENDIX A: MOS2 TIMING MODE

Here we discuss some calibration problems that affected the MOS2 spectrum, which was not considered in the spectroscopy of RXJ0059.2–7138. Note however that these issues have no impact on the timing analysis, which was indeed performed using also MOS2 events.

Source counts in MOS2 timing mode were initially extracted from RAWX=290 to RAWX=321, resulting in a count rate  $\sim 5 \text{ count s}^{-1}$ . Background was taken from an outer CCD that collected data in imaging mode. When compared with the spectra extracted from the other cameras, MOS2 spectrum showed a significant deficit of counts above 7 keV, a shortage becoming much less evident when extracting counts from a box excising the central columns of the PSF (that peaks at RAWX=305). We extracted different spectra from boxes with a variable number of excluded inner columns. For each box region, we also tried different PATTERN (single-pixel events or single and double events), but this led to a marginal difference in the resulting spectral shape in the energy range 0.6–10 keV. We followed the procedure recommended on the *XMM-Newton* SAS User Guide (issue 10.5, updated to 2014, February 7) available at [HTTP://XMM2.ESAC.ESA.INT/DOCS/DOCUMENTS/](http://xmm2.esac.esa.int/docs/documents/) to properly calculate the effective area associated with a spectrum extracted from the box in MOS2, from which the core columns have been excised. Comparing these several different MOS2 spectra, and fitting them with a simple power law model, we found significantly different slopes, even when restricting the spectral analysis to the safer energy range 2–7 keV. The reason for this behaviour is unclear (we



did not find anything similar reported in the SAS User Guide). In principle, the count rate is too low ( $\sim 5 \text{ count s}^{-1}$ ) to cause possible pile-up problems in MOS2, although the use of the SAS task EPAT-PLOT on MOS2 events (for both the whole spatial RAWX region and the different boxes chosen) showed a significant discrepancy in the distributions of observed and expected event shapes in the energy range 0.5–2 keV, while apparently no problems were found above 2 keV. We also noted a significant electronic noise in MOS2 image (TIME versus RAWX), with a repeating pattern in RAWX (several equally spaced “hot RAWX columns”), appearing only below 0.5 keV. It is possible that this huge noise creates significant problems in the MOS2 spectral reconstruction.

## REFERENCES

- Balucinska-Church M., McCammon D., 1992, *ApJ*, 400, 699
- Bird A. J., Coe M. J., McBride V. A., Udalski A., 2012, *MNRAS*, 423, 3663
- Coburn W., Heindl W. A., Rothschild R. E., Gruber D. E., Kreykenbohm I., Wilms J., Kretschmar P., Staubert R., 2002, *ApJ*, 580, 394
- Coe M. J., Bird A. J., Hill A. B., Ferrigno C., Esposito V., McBride V. A., Bartlett E. S., Townsend L. J., Haberl F., Udalski A., 2014, *The Astronomer’s Telegram*, 5766, 1
- Davies R. E., Pringle J. E., 1981, *MNRAS*, 196, 209
- den Herder J. W., Brinkman A. C., Kahn S. M., Branduardi-Raymont G., Thomsen K., Aarts H., Audard M., Bixler J. V. e. a., 2001, *A&A*, 365, L7
- Díaz Trigo M., Migliari S., Miller-Jones J. C. A., Guainazzi M., 2014, *A&A*, 571, A76
- Done C., Mulchaey J. S., Mushotzky R. F., Arnaud K. A., 1992, *ApJ*, 395, 275
- Galache J. L., Corbet R. H. D., Coe M. J., Laycock S., Schurch M. P. E., Markwardt C., Marshall F. E., Lochner J., 2008, *ApJS*, 177, 189
- Ghosh P., Lamb F. K., 1979, *ApJ*, 234, 296
- Haberl F., Sturm R., Ballet J., Bomans D. J., Buckley D. A. H., Coe M. J., Corbet R., Ehle M., Filipovic M. D., Gilfanov M., Hatzidimitriou D., La Palombara N., Mereghetti S., Pietsch W., Snowden S., Tiengo A., 2012, *A&A*, 545, A128
- Hickox R. C., Narayan R., Kallman T. R., 2004, *ApJ*, 614, 881
- Hilditch R. W., Howarth I. D., Harries T. J., 2005, *MNRAS*, 357, 304
- Hughes J. P., 1994, *ApJL*, 427, L25
- Kallman T. R., McCray R., 1982, *ApJS*, 50, 263
- Klus H., Ho W. C. G., Coe M. J., Corbet R. H. D., Townsend L. J., 2014, *MNRAS*, 437, 3863
- Kohno M., Yokogawa J., Koyama K., 2000, *PASJ*, 52, 299
- Krimm H. A., Barthelmy S. D., Baumgartner W., Corbet R. H. D., Cummings J., Gehrels N., Lien A. Y., Markwardt C. B., Palmer D., Sakamoto T., Stamatikos M., Ukwatta T., 2014, *The Astronomer’s Telegram*, 5756, 1
- Krimm H. A., Holland S. T., Corbet R. H. D., Pearlman A. B., Romano P., Kennea J. A., Bloom J. S., Barthelmy S. D., Baumgartner W. H., Cummings J. R., Gehrels N., Lien A. Y., Markwardt C. B., Palmer D. M., Sakamoto T., Stamatikos M., Ukwatta T. N., 2013, *ApJS*, 209, 14
- La Palombara N., Mereghetti S., 2006, *A&A*, 455, 283
- Parmar A. N., White N. E., Stella L., 1989, *ApJ*, 338, 373
- Porquet D., Dubau J., 2000, *A&AS*, 143, 495
- Schmidtke P. C., Cowley A. P., Udalski A., 2006, *AJ*, 132, 971
- Southwell K. A., Charles P. A., 1996, *MNRAS*, 281, L63
- Strüder L., Briel U., Dennerl K., Hartmann R., Kendziorra E., Meidinger N., Pfeffermann E., Reppin C., et al. 2001, *A&A*, 365, L18
- Sturm R., Haberl F., Pietsch W., Ballet J., Hatzidimitriou D., Buckley D. A. H., Coe M., Ehle M., Filipović M. D., La Palombara N., Tiengo A., 2013, *A&A*, 558, A3
- Tiengo A., Esposito P., Mereghetti S., Turolla R., Nobili L., Gastaldello F., Götz D., Israel G. L., Rea N., Stella L., Zane S., Bignami G. F., 2013, *Nature*, 500, 312
- Turner M. J. L., Abbey A., Arnaud M., Balasini M., Barbera M., Belsole E., Bennie P. J., Bernard J. P., et al. 2001, *A&A*, 365, L27
- Verner D. A., Ferland G. J., Korista K. T., Yakovlev D. G., 1996, *ApJ*, 465, 487
- Wilms J., Allen A., McCray R., 2000, *ApJ*, 542, 914

This paper has been typeset from a  $\text{\TeX}/\text{\LaTeX}$  file prepared by the author.